Journal of Physics: Conference Series **632** (2015) 012042 doi:10.1088/1742-6596/632/1/012042

Towards gamma-ray astronomy with timing arrays

M Tluczykont[5], I Astapov[8], N Barbashina[8], S Beregnev[11], A Bogdanov[4], D Bogorodskii[1], V Boreyko[9], M Brückner[2], N Budnev[1], A Chiavassa[6], O Chvalaev[1], A Dyachok[1], S Epimakhov[5], T Eremin[11], A Gafarov[1], N Gorbunov[9], V Grebenyuk[9], O Gress[1], T Gress[1], A Grinyuk[9], O Grishin[1], D Horns[5], A Ivanova[1], N Karpov[11], N Kalmykov[11], Y Kazarina[1], V Kindin[4], N Kirichkov[1], S Kiryuhin[1], R Kokoulin[4], K Kompaniets[4], E Konstantinov[1], A Korobchenko[1], E Korosteleva[11], V Kozhin[11], M Kunnas[5], L Kuzmichev[11], V Lenok[1], B Lubsandorzhiev[10], N Lubsandorzhiev[11], R Mirgazov[1], R Mirzoyan[7,1], R Monkhoev[1], R Nachtigall[5], A Pakhorukov[1], M Panasyuk[11], L Pankov[1], A Perevalov[1], A Petrukhin[4], V Platonov[1], V Poleschuk[1], M Popescu[12], E Popova[11], A Porelli[3], S Porokhovoy[9], V Prosin[11], V Ptuskin[8], V Romanov[9], G Rubtsov[10], M Rueger[2,3], E Rybov[1], V Samoliga[1], P Satunin[10], A Saunkin[1], V Savinov[1], Yu Semeney[1], B Shaibonov(junior)[10], A Silaev[11], A Silaev (junior)[11], A Skurikhin[11], M Slunecka[9], C Spiering[3], L Sveshnikova[11], V Tabolenko[1], A Tkachenko[9], L Tkachev[9], A Veslopopov[1], E Veslopopova[1], D Voronov[1], R Wischnewski[3], I Yashin[4], K Yurin[4], A Zagorodnikov[1], V Zirakashvili[8] & V Zurbanov[1]

[1]Institute of Applied Physics, Irkutsk State University, Irkutsk, Russia
[2]Institute for Computer Science, Humboldt-University Berlin, Rudower Chaussee 25, 12489 Berlin, Germany
[3]DESY, Platanenallee 6, 15738 Zeuthen, Germany
[4]National Research Nuclear University MEPhI (Moscow Engineering Physics Institute), Moscow, Russia
[5]Institut für Experimentalphysik, Luruper Chaussee 149, 22761 Hamburg, Germany
[6]Dipartimento di Fisica Generale Universiteta di Torino and INFN, Torino, Italy
[7]Werner Heisenberg Institut, Föhringer Ring 6, 80805, München, Germany
[8]IZMIRAN, Troitsk, Moscow Region, Russia
[9]Joint Institute for Nuclear Research, Joliot-Curie 6, 141980 Dubna, Moscow region, Russia
[10]Institute for Nuclear Research of the Russian Academy of Sciences 60th October Anniversary st., 7a, 117312, Moscow, Russia
[11]Skobeltsyn institute for Nuclear Physics, Lomonosov Moscow State University, 1 Leninskie gory, 119991 Moscow, Russia
[12]Institute of Space Science, Bucharest, Romania

E-mail: martin.tluczykont@physik.uni-hamburg.de

Abstract. The gamma-ray energy regime beyond 10 TeV is crucial for the search for the most energetic Galactic accelerators. The energy spectra of most known gamma-ray emitters only reach up to few 10s of TeV, with 80 TeV from the Crab Nebula being the highest energy so far observed significantly. Uncovering their spectral shape up to few 100 TeV could answer the question whether some of these objects are cosmic ray Pevatrons, i.e. Galactic PeV accelerators.

Sensitive observations in this energy range and beyond require very large effective detector areas of several 10s to 100 square-km. While imaging air Cherenkov telescopes have proven to be the instruments of choice in the GeV to TeV energy range, very large area telescope arrays are limited by the number of required readout channels per instrumented square-km (due to the large number of channels per telescope). Alternatively, the shower-front sampling technique allows to instrument large effective areas and also naturally provides large viewing angles of the instrument. Solely measuring the shower front light density and timing (hence timing-arrays), the primary particle properties are reconstructed on the basis of the measured lateral density function and the shower front arrival times. This presentation gives an overview of the technique, its goals, and future perspective.

1. Introduction

At its beginning, the main astrophysical motivation for gamma-ray astronomy was the search for Galactic cosmic ray accelerators. The current generation of major air Cherenkov telescopes reach down to an integral flux detection sensitivity for point sources of about $10^{-12}\mathrm{erg\,cm^{-2}\,s^{-1}}$ in the TeV energy regime after 50 h of observaton time. This lead to the discovery of many new sources of different object types in the past decade. However, the question of the origin of cosmic rays is not solved yet. While many supernova remnants (the prime candidates for cosmic ray acceleration) were detected in the TeV regime, in most cases it remains unclear whether the observed gamma-ray emission originates from cosmic ray induced hadronic processes (π^0-decay), and leptonic emission scenarios cannot be excluded (see e.g. [1]). Some of the known sources today were observed up to few 10s of TeV, partly exhibiting hard powerlaw spectra close to a differential index of -2. A measurement of the continuation of these energy spectra towards higher energies not covered by current generation instruments will help understanding the underlying acceleration mechanism of the sources. Furthermore, it remains to be seen if these objects can accelerate cosmic rays up to the (presumably) highest energies of Galactic accelerators (up to 10^{17} eV). A detection of hard gamma-ray spectra up to few 100 TeV and with an exponential cutoff that can be approximated by the form $\exp(-\sqrt{E_\gamma/300\,TeV})$ would represent a smoking-gun signature of the acceleration of cosmic rays up to the knee-feature in the all-particle cosmic ray spectrum ($E_p \approx 3 \cdot 10^{15}$ eV). Such Galactic PeV accelerators, or Pevatrons [2], have not been detected up to now. Beyond the knee-feature, in the energy range from 10^{17}-10^{18} eV, a transition is commonly believed to occur from a Galactic origin to an extragalactic origin of cosmic rays. While a detection of gamma-rays at several 10 TeV to few 100 TeV from extragalactic objects is challenging (absorption by pair-production of gamma-rays in low energy photon fields), such observations also bear potential for an indirect measurement of the extragalactic background light in the 10 μm wavelength range.

Due to the typical powerlaw shape of the energy spectra of cosmic gamma-ray sources, large effective detection areas are needed in order to access higher energies. Accessing the energy range from 10 TeV up to several 100 TeV requires an area of the order of 10 $\mathrm{km^2}$, or more. The Cherenkov Telescope Array (CTA) [3] is planned to extend the energy range up to 100 TeV and to push down the point-source detection sensitivity to few times $10^{-14}\mathrm{erg\,cm^{-2}\,s^{-1}}$ in the TeV range. However, CTA is optimized for TeV energies and will suffer from its limited collection area above 100 TeV. Even the strongest sources are expected to exhibit only few gamma-ray photons per $\mathrm{km^2}$ per year above 100 TeV, making spectroscopic studies a difficult proposition.

The non-imaging air Cherenkov technique is a complementary approach which allows larger collection areas of several square kilometers at a comparatively moderate cost in number of read-out channels. Its operating principle is based on the sampling of the density and timing (arrival-time and spread) of the Cherenkov photons from the air-shower front with distributed arrays of detector stations. Basically, this shower front sampling method is not limited to the

air Cherenkov technique, but can also be done with different detector types using the secondary shower particles, their fluorescence light, or radio emission. An overview of the most relevant parameters of different detection techniques is given in Table 1.

Table 1. Comparison between different shower-front sampling techniques. For each method, approximate values are given for the following parameters: energy threshold E_{thr}, angular resolution $\Delta\theta/\theta$, energy resolution $\Delta E/E$, quality factor of gamma-hadron separation $Q_{\gamma/h} = \epsilon_\gamma/\sqrt{\epsilon_h}$ (with the gamma-ray and hadron survival probabilities after cuts ϵ_γ, ϵ_h), and the duty cycle. A comparison between the methods always depends on the precise setup, detector multiplicity, and location of the experiment. For the sake of simplicity and in order to give an overview, only approximate typical values are given here for representative experiments such as Tibet air shower array, KASCADE-Grande, HAWC (water Cherenkov), CTA, Pierre-Auger Observatory (Fluorescence).

Method	E_{thr}	$\Delta\theta/\theta$	$\Delta E/E$	$Q_{\gamma/h}$	Duty cycle
Particles/Scintillator	3 TeV	$\sim 1^\circ$	20-50 %	~ 1	100 %
Particles/Water-Cherenkov	100 GeV	$\sim 0.5^\circ$	30-50 %	~ 6	100 %
Air Cherenkov imaging	5 GeV	$\sim 0.1^\circ$	10-15 %	~ 6	10 %
Air Cherenkov timing	10 TeV	$\sim 0.1^\circ$	10-15 %	$\sim$ 1.5-2	10 %
Fluorescence	10^{17} eV	$>1^\circ$	10-15 %	?	10 %
Radio	10^{17} eV	$<1^\circ$	10-15 %	?	100 %

Precise angular reconstruction is a key-ingredient for gamma-ray *astronomy*, and is only possible with precise timing. The particle shower front has a disk width of 30 ns at 100 m distance to the core. With less than 10 ns, the air Cherenkov photon disk width is much smaller, justifying the name *timing arrays* for air Cherenkov detectors that make use of the timing information. Further requirements of γ-ray astronomy are a good energy-resolution, a low energy-threshold, and good γ-hadron separation power, leading us back to the air Cherenkov technique as the method of choice for γ-ray astronomy with timing arrays.

While in principle, imaging air Cherenkov telescopes can also use the timing information of the Cherenkov photon arrival, their reconstruction power stems from the analysis of the air-shower image. A comparison of the imaging and timing air Cherenkov techniques in Table 2 makes clear that both techniques are complementary to each other, measuring partly independent air shower properties. A further notable difference between both techniques is that timing arrays

Table 2. Comparison of observables used for reconstruction of direction, energy and particle type for Imaging air Cherenkov telescopes and for timing arrays. Both methods are largely complementary to each other.

	Imaging	Timing
Direction	Air shower image orientation	Air shower front arrival times
Energy	Total light in image	Total light collected on ground
Particle type	Image shape	Lateral density function
		Time width & arrival times

are detectors with a large field of view (FOV) which are ideal for source surveys, but which come

at the cost of a reduced signal-to noise ratio and high energy threshold. Imaging telescopes have a small FOV, and much larger light collection area (i.e. mirror area), resulting in low noise levels per pixel and a low energy threshold.

Early on, experiments such as Jakutsk [4], Themistocle [5], or AIROBICC [6], have made first attempts to use timing arrays for γ-ray astronomy. Due to their small effective areas, these experiments could not reach the sensitivity level required for the detection of γ-ray sources in the multi-TeV energy range. Today, the Tunka-133 [7] array operates as a timing array designed for cosmic ray astrophysics. Each Tunka-133 station consists of a PMT inside a cylindrical box, covering a field of view of 50° half-opening angle. 7 such stations are connected in a cluster with a distance of 80 m between the stations. Based on a similar detection principle but a different detector design, the HiSCORE (Hundred*i Square-km Cosmic ORigin Explorer) concept [8] aims at optimizing the timing-array technique for dedication to γ-ray astronomy beyond 10 TeV. The main design differences are a factor 16 larger light collection area per station (4 PMTs with light concentrators per station, lowering the energy threshold), and fast electronics with digitization in the GHz regime. The HiSCORE detector concept was recently implemented for the first time within the Tunka-HiSCORE experiment in the Tunka-valley in Siberia. This experiment has now evolved into the TAIGA collaboration (Tunka Advanced Instrument for Gamma-ray and cosmic ray Astrophysics, also see [9], this conference), which aims at combining a timing-array with imaging telescopes. In future, also particle detectors for the measurement of the muonic component of the shower are planned.

2. The HiSCORE concept

2.1. The detector

HiSCORE is a concept for a distributed large-area (up to 100 km^2) array of wide-angle (0.6 sr) air Cherenkov detector stations covering the gamma-ray energy range from 10 TeV to several PeV, and cosmic ray physics beyond 100 TeV [8]. Important questions of astroparticle and particle physics can be addressed by air shower observations with such an array [10], the most important question being the abovementioned search for the Galactic cosmic ray Pevatrons. Each detector station consists of 4×8 inch photomultiplier tubes (PMTs), each equipped with a 40 cm diameter light concentrator (Winston cone) with a half opening angle of 30°. The effective solid angle of one station was computed taking into account the Winston cone efficiency by integrating the solid angle weighted with the zenith angle dependent Winston cone transmission probability, resulting in 0.6 sr. With 4 channels (one channel = PMT+cone), the total light collection area of one station adds up to 0.5 m^2. The resulting station threshold allows to detect a 100 TeV γ-ray air shower in the outer part of its lateral light density function (LDF) up to 350 m from the shower core impact position. The station multiplicity (number of stations in one event) is the one parameter with the strongest impact on reconstruction quality. For a given choice of the distance between detector stations, the energy threshold at reconstruction level (station multiplicity > 3) can be inferred from the LDF. In [11], the LDF parametrization takes the form of an exponential function in the inner part (typically the inner 120 m) and a powerlaw in the outer part (> 120 m) of the LDF

$$\mathrm{LDF}(r) = \begin{cases} p \exp(d\, r) & (r < 120\,\mathrm{m}) \\ q\, r^k & (r > 120\,\mathrm{m}) \end{cases} \tag{1}$$

where p and q are scaling factors. Using the most straight-forward station distribution in a regular square grid with a distance of 150 m between detector stations (referred to as standard-configuration see Figure 8) results in an average distance of ≈ 100 m between the air shower core and a station. When assuming a primary γ-ray energy of 50 TeV, on average 3 stations are expected to trigger within the inner 120 m of the LDF (see [8]). The good quality reconstruction-level threshold of such a configuration can therefore be defined to be of the order of 50 TeV.

Below this energy, events are still detected and successfully reconstructed - at lower performance, however, as illustrated by the dropping effective area (Figure 10, Section 2.4) and deteriorating angular resolution (Figure 11). Adopting a more classical definition of the energy threshold as the energy at which 50% of the effective area is reached, results in a value of about 30 TeV for the standard configuration. A further discussion of the energy threshold is given in Section 2.4. In order to obtain a large dynamic range in energy, one or two PMT-dynodes can be read out in addition to the anode. The station trigger is built using the sum of the 4 clipped analog signals in each station. The signal clipping prior to summing allows to suppress strong upward contributions of individual channels from uncorrelated night-sky background (NSB) induced signals. As opposed to NSB photons, the Cherenkov light from an air shower is - to a good approximation - distributed equally over the 4 detector station channels. The amplitude of the sum of the clipped signals is required to be above a given threshold in mV during 7 ns to issue a trigger. The chosen threshold corresponds to a voltage equivalent to 100 p.e.. This condition results in an effective signal threshold of 180 p.e. for the amplitude of the Cherenkov pulse. The readout system is based on fast analog electronics in the GHz regime, allowing to resolve the Cherenkov light pulse with at least 10 samplings (close to the core) and more than 100 samplings far from the core. Further details on the detector concept and a full detector simulation were presented in [8].

2.2. Reconstruction techniques

Methods for γ-ray and cosmic ray data reconstruction for a HiSCORE detector were presented in [11]. The basic underlying techniques described there follow the same basic principles as methods presented earlier in [7] for the Tunka-133 cosmic-ray array. The observables are the Cherenkov light density and its time-distribution measured at the individual detector stations. Figure 1 shows a Cherenkov photon arrival time distribution for a station at a distance of 200 m from the shower core of a 500 TeV simulated γ-ray air shower. The basic reconstruction parameters

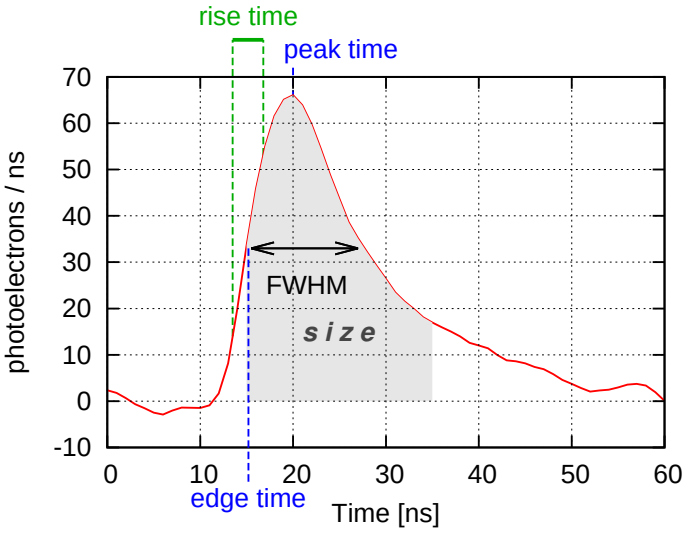

Figure 1. The simulated Cherenkov light pulse of a 500 TeV γ-ray recorded by a HiSCORE detector station in a distance of 200 m from the shower core. Simulated signal assuming a FWHM of 7 ns for the single-photo-electron response, and including noise fluctuations from light of the night-sky background. Source: [11].

are the 50 % pulse edge time, the pulse rise time (from 20 % to 80 %), the pulse amplitude, and the time integrated light signal (sometimes called the size of the pulse).

The direction is reconstructed by a fit of detector station arrival times to a model of the shape of the air shower front. Phenomenological air shower front parametrizations as well as

analytical models of the Cherenkov arrival times can be used here. As shown in [11], a relative inter-station time-calibration of better than 1 ns is required in order to limit the impact of the time-resolution on the reconstruction quality.

A first approximation for the shower core impact position is obtained from the center of gravity of the measured light distribution. For a station multiplicity of more than 5, a fit of data to a lateral density function parametrization such as given in Equation 1 yields better results.

The fitted LDF can also be used as an estimate of the total light arriving at the observation level. While the slope of the LDF depends on the shower depth, this dependency is minimal around distances of 200 m from the shower core. The value of the LDF at 220 m is used as energy estimator in [11]. A similar approach is used by [7], where the LDF value at 175 m was chosen. For spectral reconstruction, a normalization method is used based on the steepness of the LDF and a reference spectrum [12]. This method uses the logarithm of the shower-size/energy ratio which was shown to be proportional to the steepness of the LDF, i.e. the ratio between the functional value of the LDF at 100 m (Q_{100}) and its value at 200 m (Q_{200}), as illustraded Figure 2. The observed proportionality does not show a significant dependency

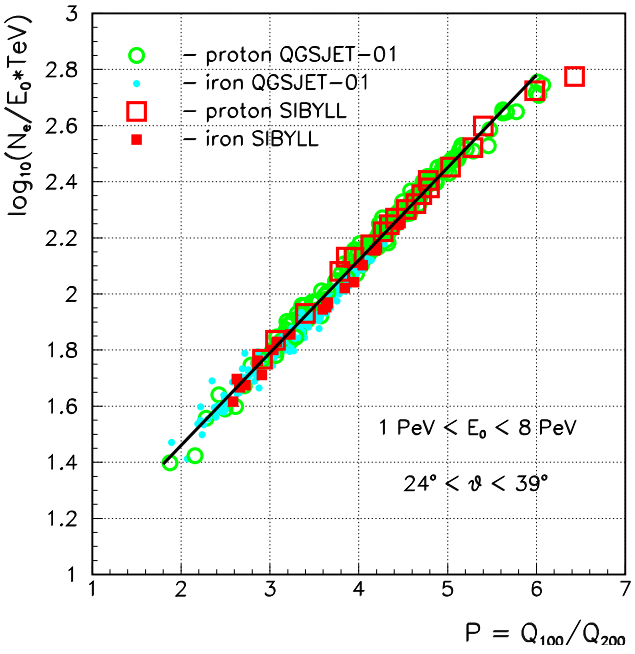

Figure 2. Proportionality between the logarithm of the shower-size/energy ratio and the steepness of the LDF, given by the ratio of its values at 100 m and 200 m from the shower core. Using this proportionality, the primary energy can be reconstructed using the measurement of the shower size and the steepness of the LDF. Source: [7].

on the used interaction model or the simulated hadronic particle type. In order to take into account variations in the light yield of the detector array and atmospheric conditions at the Tunka site, the integral energy spectrum of recorded cosmic rays is normalized to a reference spectrum previously obtained by the QUEST experiment [12].

Air showers initiated by heavier primaries develop their maximum at a smaller shower depth than lighter primaries of identical energy. Therefore, the measured shower depth as a function of the air shower energy can be used for particle separation. Methods for depth reconstruction are based on the ratio of normalization between the inner and outer part of the LDF, or on the FWHM of the time distribution of the Cherenkov light pulse as a function of the shower core impact position. The latter dependency is illustrated in Figure 3.

In a hadron induced air shower, many secondary hadrons are produced which can move further down the axis of shower development, overtaking the Cherenkov front and refueling the

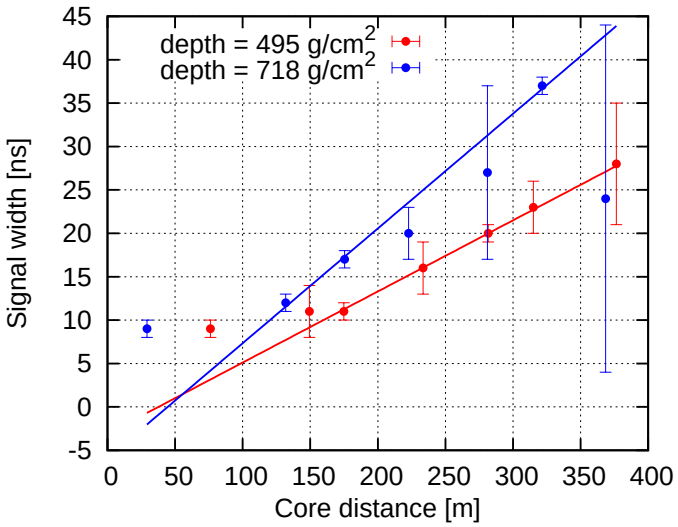

Figure 3. Signal widths (FWHM) versus core distance reconstructed from simulated data with different depths of the shower maximum. The slope of linear fits beyond 150 m core distance is used to reconstruct the depth of the shower maximum. Source: [11].

electromagnetic cascade deeper in the Atmosphere. The resulting Cherenkov light from these subshowers arrives earlier than the bulk Cherenkov light, effectively increasing the rise-time of the pulse. As shown in Figure 4 this effect can be used to a certain degree for γ-hadron separation.

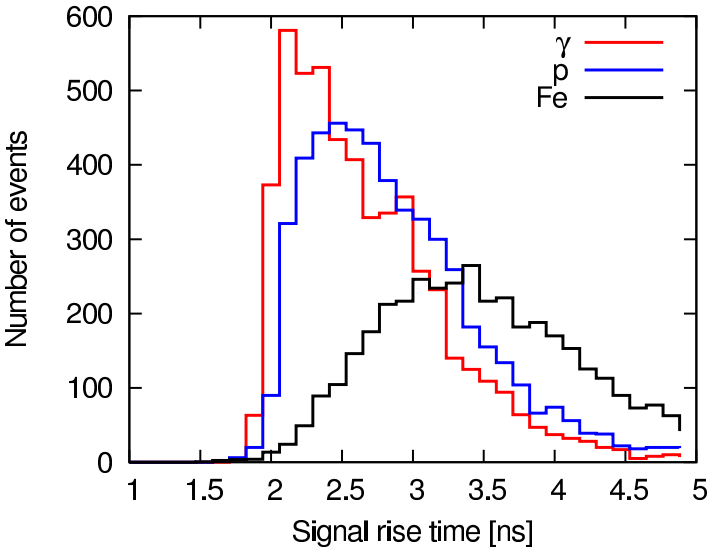

Figure 4. Rise-time distributions for γ-rays, protons and iron nuclei. The difference in rise-time is due to secondary hadrons that overtake the Cherenkov front and refuel the electromagnetic cascade deeper in the atmosphere. Source: [11].

A combination of the γ-hadron separation methods mentioned here results in an overall quality factor for γ-hadron separation of up to 2 at high energies. The reconstruction quality obtained for γ-rays in [7] is summarized in Table 3.

Table 3. Summary of reconstruction quality for the standard configuration HiSCORE array (simple regular grid, 150 m) at different energies.

	100 TeV	300 TeV	1 PeV
angular resolution	0.35°	0.1°	<0.1°
energy resolution	20 %	10 %	<10 %
Xmax resolution	70 g/cm^2	50 g/cm^2	30 g/cm^2
$Q_{\gamma/h}$	1.2	1.5	2.0

2.3. Sensitivity to γ-rays

Effective areas were calculated after acceptance cuts (reconstructed angle less than 25°, core impact contained inside array), reconstruction, and γ-hadron separation cuts. Using these effective areas and a parametrization of the expected cosmic ray background, the point-source sensitivity to γ-rays was calculated. In Figure 5 the sensitivity is shown for a 100 km^2 array after 1000 h of observation time. The shown sensitivity curve was obtained using a regular

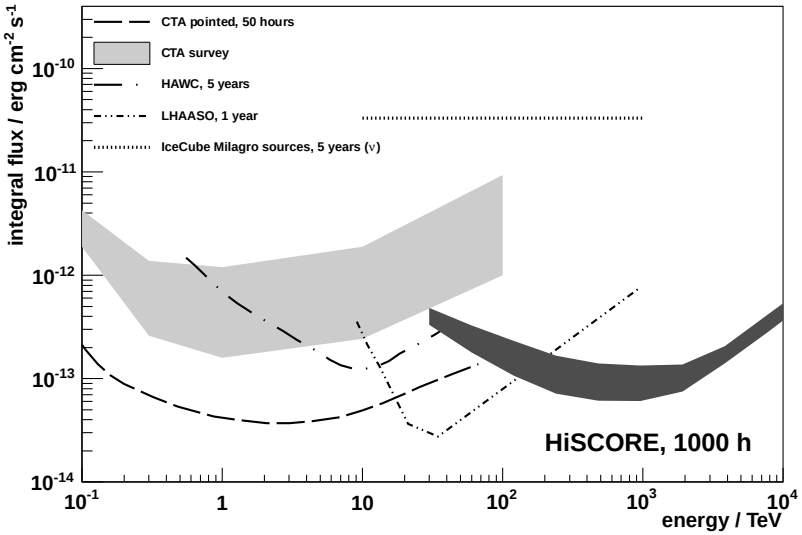

Figure 5. Point-source survey sensitivity of a 100 km^2 HiSCORE array after 1000 h of observation time (dark grey area). For comparison, the point-source *survey* sensitivities of CTA [13], of a search for neutrinos by IceCube [14] (Milagro source stacking), HAWC [15], and LHAASO [16, 17] (adapted to a minimum of 50 gamma-rays) are shown. For reference, also the 50-hour *pointed-observation* sensitivity of CTA [18] is given. Source: [8].

grid of detector stations with a spacing of 150 m between stations, shown in Figure 8. For illustration, this Figure also shows the footprint of the detected Cherenkov light of a simulated gamma-ray event. The grey-scale indicates the Cherenkov photon density in arbitrary units. A comparison of the sensitivity curve with other instruments, especially to pointing instruments, is not straight forward. A wide-angle instrument such as HiSCORE always operates in *survey mode*, with exposure accumulating for all objects visible during darkness time within the visible cone of the instrument. The accumulated exposure time for a given position is derived for event directions within 25° of the zenith [19]. The sky coverage is determined by the location of the

detector on Earth. For a northern detector site at the latitude of the Tunka-133 cosmic ray array an exposure depth of up to 400 h per source in the FOV is reached over one year, as illustrated in Figure 6. The total sky covered in one year at more than 200 h of observation time is of the order of π sr. Observations in *tilting mode* are foreseen, where all detector stations

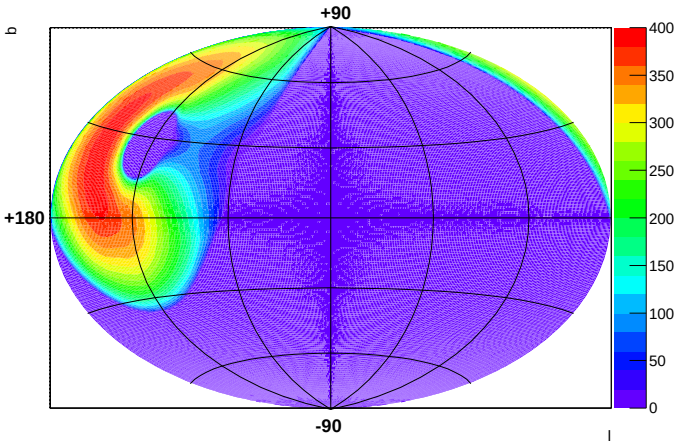

Figure 6. Sky exposure in hours and Galactic coordinates after one year of observation time at a northern site (Tunka-133 experiment site). the deepest exposures in this observation mode reach 400 h per source.

are inclined in declination towards the north or south, therewith acessing different regions of the sky at different exposure times. A schematical representation of the station tilting is shown in Figure 7. When located at a northern site, tilting towards the north results in a deeper average exposure per source while at the same time reducing the total sky coverage. Tilting towards south results in a smaller average exposure but in a large total sky coverage. For illustration, the tilted south exposure times are shown in Figure 7 for a tilting angle of 25° south at the same observation site. In the tilting south mode, the Crab-Nebula is accessed at an exposure depth

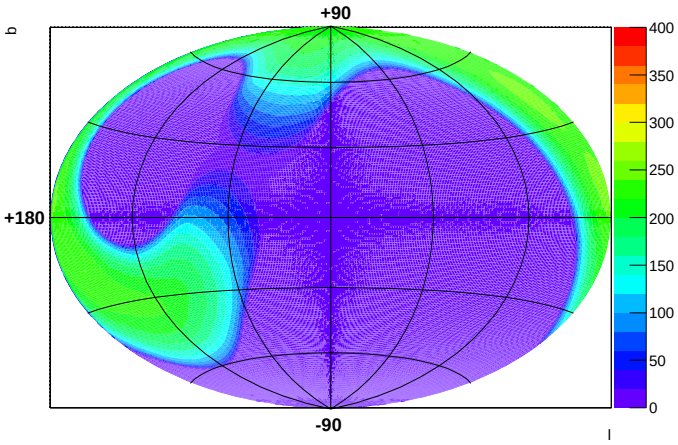

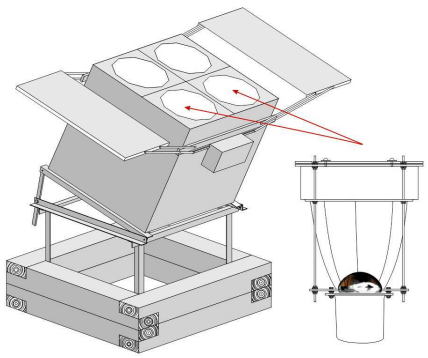

Figure 7. Left: the exposure reached at the Tunka-133 detector site for observations in the tilted south mode. Right: schematical description of the station tilting.

after efficiency correction for weather effects of more than 110 h per year at this observation site.

2.4. Optimization of array design

Alternatively, the stations can be distributed in a graded array (see Figure 9) with small inter-station distances in the center and progressively wider distances towards the edge. Such a

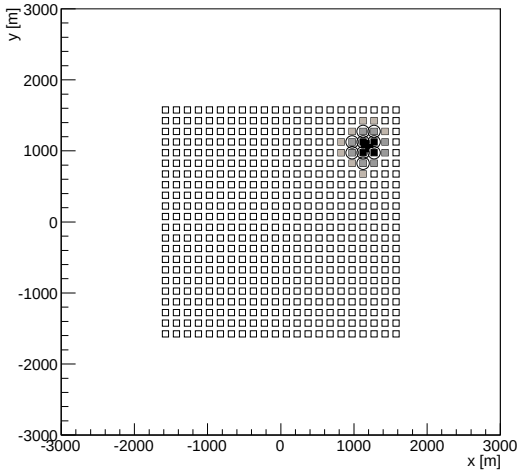

Figure 8. Station layout (484 stations) used in sensitivity calculations, and referred to as *standard layout* in the text. This array covers 10 km^2.

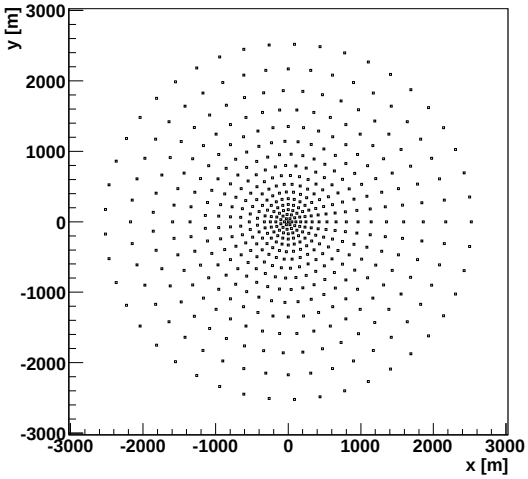

Figure 9. Geometry of a graded array (493 stations) with an instrumented area of 20 km^2 [8]. The gain in area is a factor of 2 with almost identical station numbers.

geometry is of benefit over the whole energy range. At low energies, the low inter-station distances maximize the station multiplicity (improving the angular resolution and reconstruction quality at threshold). At high energies, the larger spacing towards the edge of the array maximizes the instrumented area (compensating the rapidly decreasing γ-ray fluxes).

Using the graded array geometry, the instrumented area is a factor of 2 larger than the standard configuration (regular grid, 150 m spacing) for the same number of stations (Figure 10). At the same time, the close spacing in the inner part of the graded array allows to access lower energies, reducing the energy threshold.

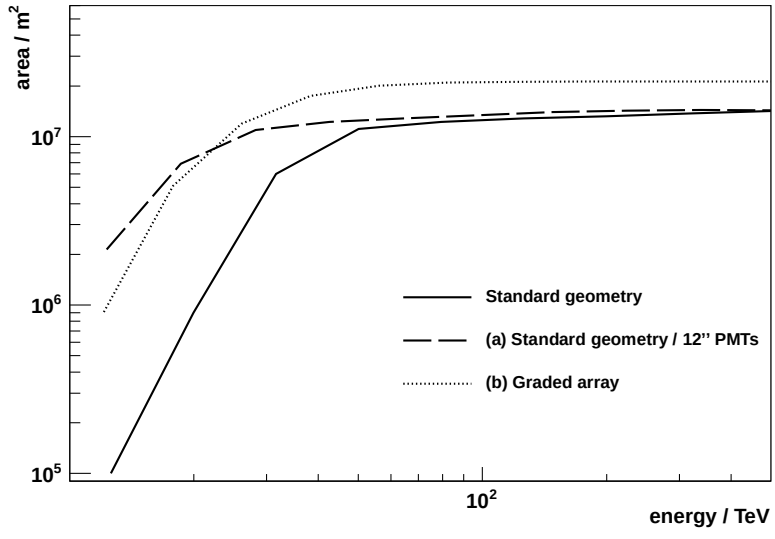

Figure 10. Effective detection area of the standard configuration as compared with two alternative layouts: (a) replacing 8 inch with 12 inch PMTs, (b) graded array. While equipping all stations with 12 inch PMTs is a costly proposition, the graded array design allows both, a gain in area (factor 2) and a lower energy threshold. Source: [8]

The effect of the higher station multiplicities of the graded array for low energies is also visible in Figure 11 showing an improved angular resolution below 300 TeV. Above this energy, the resolution deteriorates slightly, because a large fraction of high energy events are reconstructed

closer to the edge of the array, where large spacings result in decreasing station multiplicities as compared to the standard layout. The potential for improvement when using larger PMTs (also

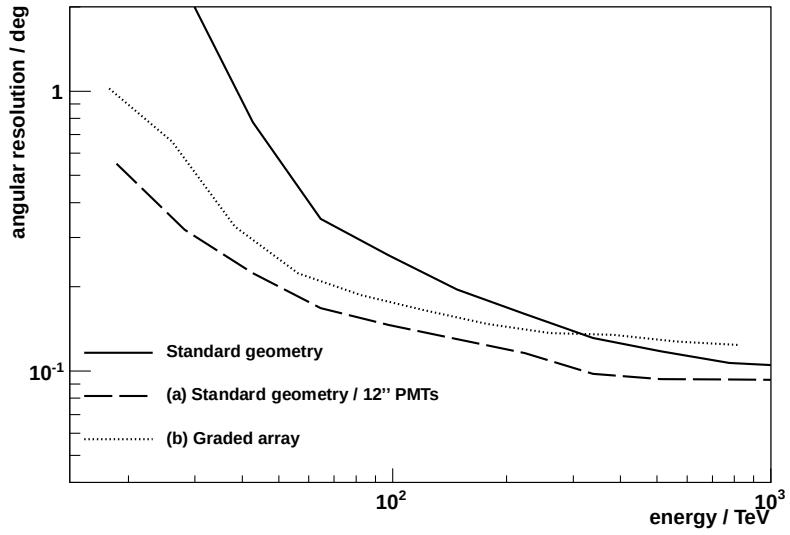

Figure 11. Angular resolution of the standard configuration array layout as compared with two alternative layouts: (a) replacing 8 inch with 12 inch PMTs, (b) graded array. The effect of the improved station multiplicity due to small inter-station distances in the central part of the array is clearly seen at low energies Source: [8]

equipped with larger Winston cones) is also shown in these Figures. However, while the graded array comes at practically no additional cost, larger PMTs do.

2.5. Minimization of Energy threshold

In the previous Section, the influence of the array layout and the choice of large area PMTs is illustrated. In this Section, we discuss the minimum achievable threshold and limiting aspects of its minimization. The energy threshold is mainly influenced by the choice of the individual station thresholds (Cherenkov light density), the array geometry (station multiplicity), and the height of the observation level. An observation site located at higher altitudes places the observer closer to the air shower, reducing the absorption of Cherenkov photons in the atmosphere. Due to the conical emission of Cherenkov light, a higher altitude also means a smaller light pool extension. On the one hand this increases the Cherenkov photon density, on the other hand a smaller light pool also reduces the station multiplicity per event. Simulations at higher altitudes show that a benefit at low energies is only achieved when using a smaller inter-station spacing, and thus a smaller overall instrumented area [19].

For a given array geometry, the lowest achievable energy threshold of the individual detector stations will optimize the energy threshold of the array and maximize the reconstruction quality (station multiplicity). The station energy threshold is limited by the imperative that the station signals be distinguishable from the noise fluctuations.

The number of photoelectrons generated by a Cherenkov pulse with photon density ρ is given by

$$N_{\mathrm{Cherenkov}} = \rho\, A\, \epsilon,$$

where A is the detector area ($0.5\,\mathrm{m}^2$), and ϵ is the efficiency of the system, including the transmission through the entrance window, the Winston cone, and the PMT quantum efficiency ($\epsilon \approx 0.14$). The number of photoelectrons generated in one station by uncorrelated NSB photons with a flux of $\phi = 3 \times 10^{12}\,\mathrm{photons\,m^{-2}\,s^{-1}}$ is given by

$$N_{\mathrm{NSB}} = \phi\, A\, t\, \Omega\, \epsilon,$$

where $\Omega = 0.6\,\mathrm{sr}$ is the effective solid angle of the detector station. Assuming the NSB in the 4 individual channels is uncorrelated, the noise fluctuations of the analog sum are given by

$$\sigma_{\mathrm{NSB}} = \sqrt{\phi\, A\, t\, \Omega\, \epsilon}.$$

Here, the time t is the noise integration time, which can be set to the length of the Cherenkov pulse. For the inner 100 m of the LDF t is less than 10 ns. However, this value has an experimental minimum value, due to the pre-amplifier response shape. A fast preamplifier can be preferable since it allows a shorter integration time t which would allow to set a shorter time-over-threshold trigger condition. On the other hand, setting a too short time would limit the sensitivity in the outer part of the LDF, since the signal time width rises with the core impact distance.

The signal-to-noise ratio is defined as $S/N = N_{\mathrm{Cherenkov}}/\sigma_{\mathrm{NSB}} = N_{\mathrm{Cherenkov}}/\sqrt{N_{\mathrm{NSB}}}$. Requiring $S/N = 3$ at threshold, results in a station threshold of 100 p.e., and a minimum detectable Cherenkov photon flux of $\rho_{thr} = 1500\,\mathrm{photons\,m^{-2}}$. This value corresponds to the light density of a 10 TeV air shower at a distance of 100 m from the shower core. For air showers at less than 100 m from the detector station, the resulting station energy threshold is lower than 10 TeV. Note that the effective event reconstruction threshold is defined at a station multiplicity of 3 and therefore strongly depends on the chosen array geometry. Consequently, when choosing a graded array layout with higher station densities in the central part of the array, the reconstruction threshold can be pushed down to the aimed at value of 10 TeV.

A practical limitation is imposed by the dead-time of the system, which rises with rising trigger rate, i.e. with lower energy thresholds. The goal must therefore be to build a read-out system which is capable of handling large data rates at minimal dead-time. After receiving the data in a central processing farm (small PC-farm), an online filtering system can provide a second stage trigger, allowing to reduce the data-flow, i.e. the size of the stored raw data. The most efficient way to reduce data flow without loss of air shower events is the requirement of a next-neighbour trigger within a given time-window. Air showers can only be reconstructed with at least 3 stations in one event. Therefore, requiring 3 neighbouring stations during online-filtering does not affect the detection rate of good air shower events while at the same time reducing the night-sky background induced trigger rate by several orders of magnitude.

3. Tunka-HiSCORE

Since 2013, Tunka-HiSCORE operates a 9-station prototype array in the Tunka-valley in Siberia, on the same site as the Tunka-133 cosmic ray array. The current array of 9 detector stations is arranged on a regular grid of 3x3 stations, with a side length of 300 m (see Figure12). Each individual detector station is built following the description in section 2. Currently, Hamamatsu 10-stage PMTs are used. In order to reduce the current due to night-sky background, the gain is limited by short-circuiting the last 3 dynode stages with the anode, effectively reducing the number of stages to 6. In the next extension, PMTs with only 6 stages will be used (ElectronTubes). Each PMT is equipped with an individual Winston cone built from segments of lightweight reflective sheets (Alanod 4300UP). The analog signals of the 4 PMT channels (only anode signals) of each station are fed into an analog summator/fan-in/fan-out module. This summator board sums the analog signals of the anodes and provides 6 output signals: the 4 analog anode signals, the signal sum, and the sum of the clipped signals. Currently, the signal sum is used for triggering. In future also the clipped signal sum will be used. At this stage of the experiment, two parallel DAQ systems were installed in all 9 stations. The first DAQ system [9] uses an analog sampling board based on the Domino Ring Sampler (DRS 4) chip, using 8 channels for signal sampling. A 9th channel is used for time calibration using a clock signal sent over separate fibers. Data are read out using an Xilinx evaluation board and sent via an optical fibre ethernet link to a central DAQ-PC. The second DAQ system [20] is based

on the DRS 4 evaluation board, coupled with a raspberryPI mini-PC, and the WhiteRabbit time-synchronization (time-synchronization and GBit data over a single monomode fiber) [21]. The raspberryPI reads out the DRS 4 evaluation board and sets one of its onboard I/O pins to *high*, signalling readiness for the next trigger to the WhiteRabbit board. The latter is generating the trigger from the analog sum using its FPGA module. After readout, the raspberryPI sends data via optical fibre link to a central DAQ-PC. The previously mentioned crucial requirement of sub-ns relative precision of time-synchronization between stations was achieved with both DAQ and synchronization systems (see [21] and [9]). A recent study presented in [20] uses the residuals of the fit of an air-shower front arrival time model to data to estimate the relative time synchronization between stations, yielding a resolution of 0.6 ns.

The array geometry planned to be completed until 2015 is shown in Figure 13. With the additional stations (shown in red) in total 34 stations will be in operation, covering an area of about 0.25 km^2.

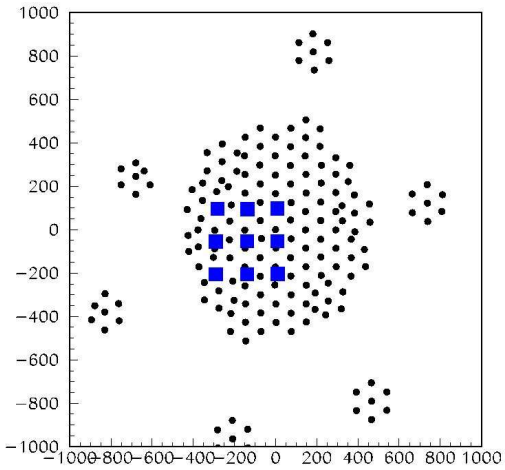

Figure 12. Station layout of the Tunka-HiSCORE 9-station prototype array. The Tunka-HiSCORE detector stations (blue squares) are embedded in the Tunka-133 array (black circles), and covers a total area of roughly 0.1 km^2.

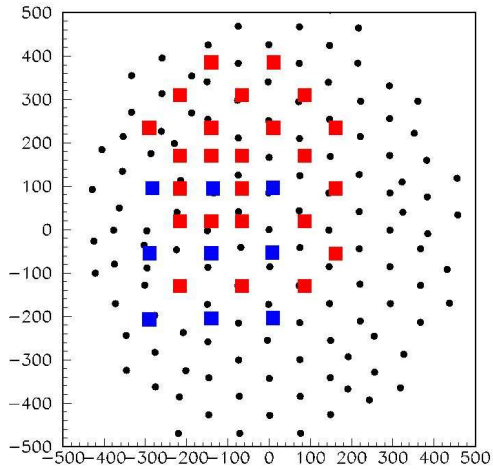

Figure 13. Planned layout for deployment in Autumn 2014. 25 additional stations (red) will reduce the station spacing in the central part of the array (increasing station multiplicity) and increase the total area covered by the array to 0.25 km^2.

4. Combining imaging and timing: TAIGA

The TAIGA experiment [9] is planning to combine the HiSCORE timing array with 10 small sized imaging air Cherenkov telescopes. Each IACT will consist of a 34-segment tesselated mirror dish in Davies-Cotton design, with a diameter of the individual mirror facets of 60 cm, a focal length of 4.75 m, a mirror dish diameter of 4.3 m, and a PMT camera. The PMTs will be arranged with a 30 mm center-to-center distance in 11 hexagonal rings around the central pixel. The energy threshold of such IACTs is predicted to be about 500 GeV. The telescopes can be exploited in different modes: (1) as stand-alone telescopes performing monitoring observations (using the classical imaging technique) of transient sources in the energy range of 500 GeV up to few 10 TeV, and providing a wide energy range for inter-calibration; (2) as integral part of the timing array, providing high-quality amplitude and shower front timing measurements;

(3) in the promising hybrid timing/imaging mode, described below. The timing stations and the individual imaging telescopes are planned to trigger independently from each other. Data merging will be performed using the synchronized (sub-ns) event time-stamps.

The basic idea for a combination of the imaging and timing techniques is to use the timing array to determine the air shower core position and the direction of the primary particle. A combination of these parameters with the image of the IACT is a promising new hybrid approach.

A large instrumented area is the key element for optimizing the array for the energy range from 10 TeV to few 100 TeV. Therefore, the telescopes will be placed at a distance of 600 m from each other. In this configuration all telescopes will operate in monoscopic mode for zenith angles up to 60°. Combining the monoscopic telescopes with the HiSCORE timing array in a hybrid array will result in an improved reconstruction and gamma-hadron separation quality as compared to monoscopic telescopes alone, as outlined below (also see [22], these proceedings).

Image scaling The width of the air shower image as measured by an IACT depends on the impact position of the air shower core, the zenith angle and the energy of the air shower event. Using Monte Carlo simulations, lookup tables can be generated for the expected width as a function of the shower core impact distance (R_c), the zenith angle (θ) and the amplitude (A, also called size) of the image (correlated with the energy), $w_{MC}(R_c, \theta, A_{\mathrm{IACT}})$. If these three parameters are known, the measured image width w_{IACT} can be scaled with the expected width:

$$scw = \frac{w_{\mathrm{IACT}}}{w_{MC}(R_c, \theta_{\mathrm{IACT}}, A_{\mathrm{IACT}})},$$

ultimately providing a means for gamma-hadron separation, since hadronic images tend to be wider than their purely electromagnetic counterparts. Typically, this scaled width parameter is used very successfully by *stereoscopic* IACT systems, which provide a good core position reconstruction (R_c), e.g. from the intersection of the image axes of two or more telescopes. Since more than one width measurement is available in stereoscopic systems, the mean of all scaled widths ($mscw$) is used.

In TAIGA however, the telescopes are planned to be placed up to 600 m apart in order to cover a very large area. Therefore, the telecopes will mainly be operating in *monoscopic* mode. Each single telescope taken alone will not be able to reliably measure the core impact for the majority of events. This is where the timing array comes into play: arranged in an array around the IACTs, the HiSCORE timing-array stations will provide their measure of the core impact position R_{HiSCORE} and direction $\theta_{\mathrm{HiSCORE}}$ to each telescope, allowing the determination of a hybrid scaled width, $hscw$, as given in Equation 2 without recurring to the stereoscopic technique

$$hscw = \frac{w_{\mathrm{IACT}}}{w_{MC}(R_{\mathrm{HiSCORE}}, \theta_{\mathrm{HiSCORE}}, A_{\mathrm{IACT}})}. \quad (2)$$

Preliminary simulations show that the gamma-hadron separation quality factor (defined as the ratio of gamma-efficiency ϵ_γ to the square-root of hadron efficiency ϵ_h) of a cut on the here-described $hscw$ parameter is $Q_{hscw} = \epsilon_\gamma/\sqrt{\epsilon_h} \geq 2$.

Image orientation In stereoscopic systems, the direction of the air shower is reconstructed following the same principle as for the core position. With the large separation of the individual TAIGA telescopes, this reconstruction technique cannot be applied and the precise unambiguous directional information is lost for the bulk of the telescope events. Instead, the timing array will again provide the lost information to the telescopes, resulting in a strong reduction of the background below the gamma-ray signal. Furthermore, the orientation of the elliptical shower image combined with the direction from the timing array can provide an improved directional

reconstruction as compared to the pure timing-array reconstruction. Such a combination might also provide a gamma-hadron separation criterion. The major axis from an IACT will intersect the direction of the timing array in case of gamma-rays, while in the case of hadron-induced air showers, the irregular nature of the IACT image will tend to misalign the axis.

Reconstruction quality Finally, integrating the timing and amplitude information of each individual telescope to the measurements of the timing-array will effectively add photon density and timing measurements with very good sensitivity (large mirror area). A telescope would then provide an additional high-quality amplitude measurement for the lateral density function fit, and an additional high-quality timing measurement for the arrival time fit. Overall, this will lead to an improvement of the reconstruction quality of the direction, the energy and the shower depth as compared to the reconstruction quality of the individual detector components alone.

Hybrid array sensitivity By operating the telescopes in monoscopic mode with distances of the order of 600 m between telescopes the total area covered per telescope is larger than the area that could be covered using the same number of telescopes as a stereoscopic system (requiring distances of roughly 300 m in the 10–100 TeV energy regime). This is a key aspect for acessing the energy range from 10 TeV to several 100 TeV (powerlaw spectra). The timing array alone was shown to only allow poor gamma-hadron separation at low energies (10–100 TeV), with a quality factor of the order of unity below 100 TeV and only reaching 2 above few 100s of TeV. As opposed to that, using the hybrid scaled width and image orientation as described above will provide an overall gamma-hadron separation quality of at least 2 at 10 TeV, and possibly as good as 3. The improved quality of the hybrid reconstruction (direction, energy) will also have a beneficial effect on the sensitivity in the overlapping energy range.

Between 10 TeV and 100 TeV, and for a given instrumented detector area, the angular resolution and the gamma-hadron separation are the dominant factors for the point-source sensitivity shown in Figure 5. Above 250 TeV, the gamma-hadron separation alone becomes the dominant factor. Summarizing, the hybrid array reconstruction technique will allow a maximization of the area and an optimization of the sensitivity to gamma-rays above 10 TeV.

5. Summary

Accessing the gamma-ray energy range from 10 TeV to several 100 TeV with spectroscopic measurements is of prime importance for understanding the continuation of known gamma-ray sources and for the search of the Galactic cosmic ray Pevatrons. The timing-array Cherenkov technique is a promising approach for covering this energy regime at the required sensitivity level. With Tunka-HiSCORE, first steps were taken toward a timing-array dedicated to gamma-ray astronomy. Within the TAIGA collaboration, this concept will be realized on a larger scale of the order of km^2 within the coming years. With the hybrid detector concept, combining the air Cherenkov timing-array technique with the air Cherenkov imaging technique, TAIGA will deploy a unique detector, optimizing the sensitivity to gamma-rays above 10 TeV.

5.1. Acknowledgments

We acknowledge the support of the Russian Federation Ministry of Education and Science (agreements N 14.B25.31.0010, zadanie No 3.889.2014/K), the Russian Foundation for Basic research (13-02-00214, 13-02-12095, 15-02-10005, 15-02-05769), the Helmholtz association (grant HRJRG-303), and the Deutsche Forschungsgemeinschaft (grant TL 51-3).

References

[1] Morlino G, Amato E and Blasi P 2009 *MNRAS* **392** 240–250
[2] Gabici S and Aharonian F A 2007 *The Astrophysical Journal Letters* **665** L131–L134

[3] Acharya B S, Actis M, Aghajani T, Agnetta G, Aguilar J, Aharonian F, Ajello M, Akhperjanian A, Alcubierre M, Aleksić J and et al 2013 *Astroparticle Physics* **43** 3–18
[4] Dyakonov M N, Knurenko S P, Kolosov V A *et al.* 1986 *Nuclear Instruments and Methods in Physics Research A* **248** 224
[5] THEMISTOCLE Collaboration, Baillon P, Behr L, Danagoulian S *et al.* 1993 *Astroparticle Physics* **1** 341
[6] Karle A, Merck M, Plaga R *et al.* 1995 *Astroparticle Physics* **3** 321
[7] Berezhnev S F, Besson D, Budnev N M *et al.* 2012 *Nuclear Instruments and Methods in Physics Research A* **692** 98
[8] Tluczykont M, Hampf D, Horns D, Spitschan D, Kuzmichev L, Prosin V, Spiering C and Wischnewski R 2014 *Astroparticle Physics* **56** 42–53
[9] Budnev N *et al.* 2015 The Tunka experiment: from cosmic ray to gamma-ray astronomy; To appear in IOP Conference Series, ECRS 2014, Kiel, Germany (These proceedings)
[10] Tluczykont M, Hampf D, Horns D *et al.* 2011 *Advances in Space Research* **48** 1935
[11] Hampf D, Tluczykont M and Horns D 2013 *Nuclear Instruments and Methods in Physics Research A* **712** 137–146
[12] Korosteleva E E, Prosin V V, Kuzmichev L A and Navarra G 2007 *Nuclear Physics B (Proc. Supp.)* **165** 74–80
[13] Dubus G, Contreras J, Funk S *et al.* 2013 *Astroparticle Physics* **43** 317
[14] Gonzalez-Garcia M C, Halzen F and Mohapatra S 2009 *Astroparticle Physics* **31** 437
[15] Sinnis G 2005 HAWC: A Next Generation VHE All-Sky Telescope *Heidelberg Gamma-Ray Symposium* (*American Institute of Physics* vol 745) ed Aharonian F A, Völk H J and Horns D p 234
[16] Cao Z 2010 *Chinese Physics C* **34** 249
[17] Cui S, Liu Y, Liu Y and Ma X 2014 *Astroparticle Physics* **54** 86 – 92
[18] CTA Consortium, Actis M, Agnetta G, Aharonian F, Akhperjanian A *et al.* 2011 *Experimental Astronomy* **32** 193
[19] Hampf D, Tluczykont M and Horns D 2010 Simulation of the expected performance for the proposed gamma-ray detector HiSCORE proceedings of Science (Texas 2010) 245
[20] Porelli A *et al.* 2015 Timing calibration and directional reconstruction for Tunka-HiSCORE; To appear in IOP Conference Series, ECRS 2014, Kiel, Germany (These proceedings)
[21] Brückner M, Wischnewski R *et al.* 2013 Results from the whiterabbit sub-nsec time synchronization setup at hiscore-tunka; To appear in Proc. of 33RD ICRC 2013, Rio de Janeiro, Brazil
[22] Kunnas M *et al.* 2015 Simulation of the Tunka Advanced International Gamma-ray Advanced experiment (TAIGA); To appear in IOP Conference Series, ECRS 2014, Kiel, Germany (These proceedings)